Received: 26 July 2022 | Revised: 8 September 2022 | Accepted: 28 September 2022

DOI: 10.1002/ppap.202200137

RESEARCH ARTICLE

PLASMA PROCESSES AND POLYMERS

Molecular understanding of the possible mechanisms of oligosaccharide oxidation by cold plasma

Maksudbek Yusupov[1,2,3,4] | **Debbie Dewaele**[5] | **Pankaj Attri**[1,6] | **Umedjon Khalilov**[1,2,3,4] | **Frank Sobott**[5,7] | **Annemie Bogaerts**[1]

[1]PLASMANT Research group, Department of Chemistry, University of Antwerp, Universiteitsplein 1, Antwerp, 2610, Belgium

[2]School of Engineering, Akfa University, Tashkent, 111221, Uzbekistan

[3]Department of Power Supply and Renewable Energy Sources, National Research University TIIAME, Tashkent, 100000, Uzbekistan

[4]Laboratory of Thermal Physics of Multiphase Systems, Arifov Institute of Ion-Plasma and Laser Technologies, Academy of Sciences of Uzbekistan, Tashkent, 100125, Uzbekistan

[5]BAMS Research group, Department of Chemistry, University of Antwerp, Groenenborgerlaan 171, Antwerp, 2020, Belgium

[6]Center of Plasma Nano-interface Engineering, Kyushu University, Fukuoka, 819-0395, Japan

[7]School of Molecular and Cellular Biology and Astbury Centre for Structural and Molecular Biology, University of Leeds, Woodhouse Lane, Leeds, LS2 9JT, UK

Correspondence
Maksudbek Yusupov, PLASMANT Research group, Department of Chemistry, University of Antwerp, Universiteitsplein 1, Antwerp, 2610, Belgium,
Email: maksudbek.yusupov@uantwerpen.be

Funding information
Fonds Wetenschappelijk Onderzoek, Grant/Award Number: 1200219N

Abstract

Cold atmospheric plasma (CAP) is a promising technology for several medical applications, including the removal of biofilms from surfaces. However, the molecular mechanisms of CAP treatment are still poorly understood. Here we unravel the possible mechanisms of CAP-induced oxidation of oligosaccharides, employing reactive molecular dynamics simulations based on the density functional-tight binding potential. Specifically, we find that the interaction of oxygen atoms (used as CAP-generated reactive species) with cellotriose (a model system for the oligosaccharides) can break structurally important glycosidic bonds, which subsequently leads to the disruption of the oligosaccharide molecule. The overall results help to shed light on our experimental evidence for cellotriose oxidation by CAP. This study provides atomic-level insight into the onset of plasma-induced removal of biofilms, as oligosaccharides are one of the main components of biofilm.

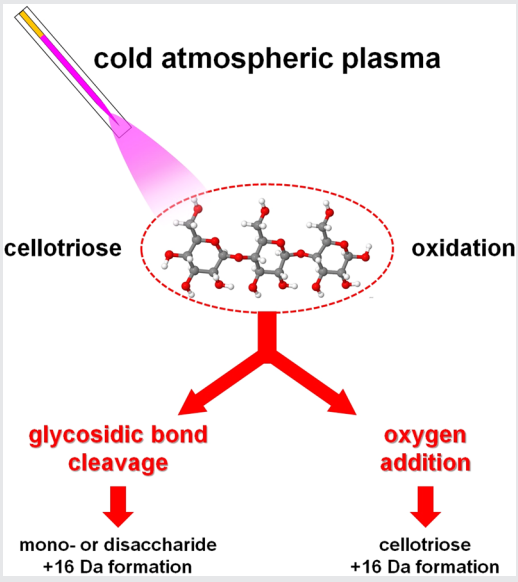

KEYWORDS
cold atmospheric plasma, oligosaccharide, plasma oxidation, reactive molecular dynamics, reactive oxygen species

1 | INTRODUCTION

The growth of biofilms causes severe problems in health-related industries.[1] Biofilms can be grown on both living and nonliving surfaces, resulting in significant concerns in hospitals and medical industries.[2,3] The growth cycle of biofilm includes bacterial adhesion at various levels, that is, it starts with the interaction of bacteria on the substrate, and it ends with the release of cell clusters from the biofilm matrix.[4,5]

Biofilm consists of proteins, nucleic acids, amino acids, and excreted polysaccharides.[6] Polysaccharides act as an extracellular polymeric substance that protects bacteria against antibiotics. Conventional sterilization methods like chemical cleaning, heating, and X-ray irradiation are used to substitute traditional treatments with antibiotics. However, these techniques do not provide the desired results, mainly for sterilization of medical equipment. Therefore, in the last few years, cold atmospheric plasma (CAP) has emerged as a useful substitute to treat biofilms.[7,8] CAP uses numerous inactivation mechanisms, such as destabilization of the biofilm communities and its matrix components (e.g., oligosaccharides) responsible for making biofilm.[9] In a recent study, air-dielectric barrier discharge (DBD) plasma was used to treat biofilms of *Escherichia coli* and *Staphylococcus aureus*.[10] After less than 4 min of DBD treatment, more than 85% of *Escherichia coli* and 70% of *Staphylococcus aureus* biofilms lost their metabolic capacity. In addition, air-DBD treatment caused significant disruption of the membranes of both biofilms.[10] In another recent study, the antimicrobial efficacy of CAP against *Streptococcus mutans* biofilms was investigated and the results were compared with those obtained using 2% chlorhexidine for treatment.[11] Counting of viable colonies (i.e., colony-forming unit [CFU]) and bioluminescence assay (BL) revealed that 150 s CAP treatment significantly reduced the CFU and BL values compared to the control, but 2% chlorhexidine showed stronger action than 150 s CAP treatment. On the other hand, there were no structural or morphological changes in the biofilm after chlorhexidine treatment, while CAP treatment showed clear signs of these changes. Additionally, DNA damage was observed after plasma treatment, which was not the case for chlorhexidine. The authors suggested that CAP treatment can be used as an intraoral surface decontamination strategy to remove the biofilm, which is different from the chemical treatment.[11]

Antibiotics have lower permeation into the biofilm matrix, thus bacteria encapsulated in the biofilm reveal high resistance to antimicrobial and antibiotics agents.[12,13] On the other hand, CAP-generated reactive species can deeply penetrate into the biofilm.[14] Moreover, secondary reactive species produced during the plasma interaction with biofilm decrease the bacterial extracellular polymeric substance thickness, which results in increased bacterial cell susceptibility to the CAP.[15] For this nonspecific mechanism of biofilm interruption and elimination of bacteria, it is difficult to develop resistance to CAP-induced oxidative stress, which can be considered an effective method against infections and bacterial pathogens.

According to pharmacopoeial sterilization, sterilization means the entire absence of microorganisms. However, a sterility assurance level (SAL) of 10^{-6} is generally accepted.[16,17] The basic premise of the SAL concept is that the inactivation of microorganisms by physical or chemical means follows first-order exponential kinetics with a linear inactivation plot.[17] A continuously decreasing probability of surviving microorganisms due to continuously increasing treatment time, with extrapolation reached to sterility guarantee level of 10^{-6}.[17] However, in the literature, CAP treatment on microorganisms shows discontinuous plots.[18,19] To determine the true form of antimicrobial inactivation kinetics, it is crucial to investigate a wide variety of sub-effective treatment times. It is practically impossible to make accurate claims about inactivation kinetics in the SAL range due to the nonlinearity of the inactivation plot in the experimentally available data range.[17] Any data extrapolation into the SAL range would therefore be extremely difficult. As a result, CAP treatments cannot ensure sterilization by pharmacopoeial criteria. Although the antimicrobial effect of CAP is well documented, the molecular mechanism is still limited due to the complexity of the biofilm. In this regard, a molecular-level understanding of the plasma effect on the biofilm components, such as polysaccharides, is crucial.

Soignet et al. reported that mono- and polysaccharides were chemically modified by an RF plasma using O_2, N_2, and Ar as feed gases.[20] The authors noted that plasma treatment results in the formation of on average

one carbonyl group per monosaccharide unit. These carbonyl groups were formed on the surface and bulk of the CAP-treated monosaccharides.[20] Li et al. showed that treating an aqueous glucose solution with dielectric barrier discharge plasma mainly leads to the formation of acids, for example, oxalic, glycolic, tartaric, glyceric, and formic acid, after various time exposure and concentrations, which were related to the reactive oxygen species (ROS) and mainly hydroxyl radicals in the liquid.[21] A similar conclusion was made in a very recent study of D-glucose oxidation by CAP-generated reactive species.[22] It was shown that short-lived species, such as hydroxyl (OH) radical and especially atomic oxygen (i.e., $O(^3P)$ radical or simply O atom), are the main reactive species involved in the glucose oxidation cascade, whereas the long-lived hydrogen peroxide (H_2O_2) is irrelevant for oxidation, that is, it is a by-product of this process. The authors also suggested that O atoms are the primary oxidants of glucose in Ar/O_2 admixture plasma with or without N_2 shielding flow.[22] A similar statement was reported in,[23] where it was shown that the O atoms can directly oxidize organic molecules, without any intermediate reactions (i.e., dissociation of water molecules) in an aqueous solution. It was mentioned that CAP can be used as an effective source of O atoms without the need for chemical precursors in the liquid phase.[23] Almeida et al. reported a decrease in oligosaccharide chain length by four to seven glycosidic-linked saccharide monomers during direct and indirect plasma treatment, similar to the CAP effect on fructose.[24] The authors suggested that direct or indirect CAP treatment causes the breakage of glycosidic bonds due to the reaction of plasma-generated reactive species.[24] Delaux et al. also showed that the CAP-generated reactive species interact with cellulose, leading to the cleavage of glycosidic bonds and the release of short-chain cellodextrins, which subsequently form branched glucans.[25] Still, these experimental data provide only a limited understanding of the effect of plasma on saccharides and do not reveal its mechanism of action at the molecular level.

In this regard, computer simulations can be a useful tool to complement experiments, as they can provide insight into processes occurring at the molecular level. There are several molecular dynamics (MD) simulation studies in the literature devoted to the investigation of the interaction of plasma-generated species with biomolecules containing at least disaccharides. In our earlier studies, we investigated the interaction of ROS (e.g., atomic oxygen [O] and hydroxyl [OH] radical) with peptidoglycan, the outer layer of the cell wall of gram-positive bacteria.[26,27] One of the main components of this biomolecule is a disaccharide (i.e., *N*-acetylglucosamine and *N*-acetylmuramic acid connected with β(1–4) glycosidic bond) repeating unit. The simulation results revealed that the interaction of ROS leads to the breaking of the glycosidic bond in the disaccharide, as well as to the opening of the rings in one of the sugar monomers.[26,27] In our subsequent study with the lipid A molecule (i.e., the endotoxic biomolecule of gram-negative bacteria), we obtained similar results with its disaccharide (i.e., two glucosamine linked with β[1–6] glycosidic bond). Upon interaction with OH radicals, the dissociation of C-O bonds as well as the formation of double C=C and C=O bonds occurred in the disaccharide, leading to the cleavage of its glycosidic bond and the opening of the sugar ring.[28,29] Khosravian et al. also observed the chemical reactions of OH radicals with the *N*-acetyl glucosamine molecule, a constituent component of *Staphylococcus epidermidis* biofilm. It was found that the reactions are initiated by H-abstraction from the molecule, which subsequently leads to the opening of its ring, as well as to its damage.[30] Similar conclusions were made by Zhao et al. when studying the interaction mechanisms of ROS (i.e., O, OH, and O_2) with β1,6-glucan, a model system for the *Candida albicans* cell wall.[31] The authors reported that O and OH species can break structurally important C-C and C-O bonds, which are induced by H-abstraction from OH or CH groups of the molecule. This subsequently triggers a cascade of bond dissociation and double bond formation events, leading for example, to the ring opening in sugar monomers.[31] In their later study with β-glucan (i.e., a model system for the *Saccharomyces cerevisiae* cell wall) as well as chitin polymer (the skeletal component of the *Candida albicans* cell wall), the same research group obtained similar results for ROS interactions.[32,33] They found that among the various ROS, the O and OH species are highly reactive and can easily break important bonds of oligosaccharides, which leads to the cleavage of glucosidic bonds.[32,33] In their other research with poly-β-1–6-*N*-acetylglucosamine (i.e., one of the important components in some biofilms), the group again observed similar results. They found that OH radicals are involved not only in H-abstraction, which can lead to the destruction of the molecular structure of the polysaccharide through dissociation of glycosidic bonds but also in OH addition to the sugar molecule.[34] Recently, Yin et al. observed that the interaction of ROS (i.e., O, OH, and H_2O_2) with cellulose polysaccharide results in a change in its chain structure, such as the formation of aldehyde and vinyl groups, as well as the reduction of the OH groups and pyran rings.[35] Note that in the above studies, the authors investigated the effect of collective impacts of ROS (including their products formed in the gas phase) on oligosaccharides. However, understanding the effect of a single ROS, e.g., O atoms, on

oligosaccharide oxidation is also important. In particular, in our recent study,[36] we revealed that the impact of O atoms leads to a ring-opening in hyaluronan oligosaccharide, which was also experimentally evidenced with periodate oxidation. [37] The ring opening in hyaluronan can subsequently lead to its degradation, thereby lowering its molecular weight.[38,39]

Thus, in the present study, we investigate the effect of a single ROS impact on a cellotriose molecule as a simple model system for oligosaccharide, one of the main components of biofilm. Specifically, we study the nonconsecutive impact of O atoms (as the most reactive ROS, but with a behavior representative for other ROS[26–28,36]) on intact cellotriose, by applying reactive MD simulations.

2 | SIMULATION DETAILS

To obtain a better insight into the effect of oxygen plasma and to provide atomic-level information on the reaction mechanisms, we performed reactive MD simulations employing the density functional-tight binding (DFTB) potential (i.e., DFTB-MD).[40] DFTB is an approximate density functional theory (DFT) method,[40] based on a Taylor series expansion of the DFT total energy expression. DFTB is two orders of magnitude faster than DFT,[41] but computationally more expensive than classical reactive MD methods such as ReaxFF-MD. However, it accurately describes the H binding energies, proton affinities, and H transfer barriers without losing its speed and robustness.[42] Moreover, it can describe resonance structures, while ReaxFF-MD cannot explicitly handle them.[43]

In this study, we used the so-called DFTB3 method, which is the extended and improved version of self-consistent charge DFTB.[42] For the description of the interatomic interactions in our DFTB-MD simulations, we employed a parameter set, called "3ob-3-1," which was specifically developed for DFTB3 and can be used for organic and bio-molecules.[44,45]

As a model system, we employed the cellotriose structure (see Figure 1 below). The structure of cellotriose trisaccharide consists of three β-D-glucose units linked via 1,4-β glycosidic bonds. We studied the interaction of cellotriose with atomic oxygen, which is one of the reactive species generated by CAP.[46] To study in detail all possible bond breaking and formation processes upon O atom impact, and to obtain some (limited) statistics, we need to perform a large number of DFTB-MD simulations. Thus, we carried out 100 DFTB-MD simulations to investigate the possible reaction mechanisms of O atom interaction with cellotriose trisaccharide. By performing a single O atom impact in each simulation, we can indeed obtain some statistics of the occurring mechanisms. It should be mentioned here that we did not consider the aqueous layer covering the cellotriose molecule. This is because of the high computational cost of the DFTB method, as modeling the system with the water layer would take an excessively long calculation time. Moreover, as mentioned in the Introduction, we investigated the effect of exclusively an O atom and its nonconsecutive impact to find out how an individual ROS (i.e., O atom) would influence the cellotriose oxidation process and how close the simulation results would be to the experimental results. Our approach used in this study (i.e., the interaction of only the O atom and the use of cellotriose without a water layer surrounding it) seems sufficiently justified since the simulation results are qualitatively in line with the experimental results (see Section 4 below).

The cellotriose molecule (containing 66 atoms, see Figure 1 below) was placed in a box with a size of 25 Å × 25 Å × 25 Å. This box size was large enough to randomly create a single O atom around the structure (see below). The geometry of the system was optimized using the conjugate gradient algorithm. The system was then equilibrated (i.e., thermalized) for 15 ps in an NVT ensemble (i.e., a system with a constant number of particles N, volume V and temperature T), at 300 K, employing the Berendsen thermostat[47] with a coupling constant of 100 fs. We used a time step of 0.5 fs in all simulations, that is, during the thermalization, as well as during the later particle impact simulations. Periodic boundary conditions were applied in all three directions. Subsequently, a single O atom was randomly created around the structure with a minimum distance of 5 Å from the molecule. This was done to avoid initial long-distance interactions between the O atom and the cellotriose molecule (i.e., Coulomb and van der Waals interactions). The impact simulations (i.e., 100 DFTB-MD runs) were performed for a total simulation time of 30 ps (i.e., 6×10^4 iterations) per simulation, which was long enough to realize bond breaking and formation in the structure. All simulations were carried out applying the DFTB + package[48,49]

3 | EXPERIMENTAL DETAILS

A micro-scale atmospheric pressure plasma jet (μ-APPJ)[46,50] was used for the oxidation of cellotriose. In this CAP source, the plasma is operated in helium with oxygen admixture (1.6%), resulting in the formation of reactive plasma species (including ROS). The ability of this plasma source to operate at ambient pressure and

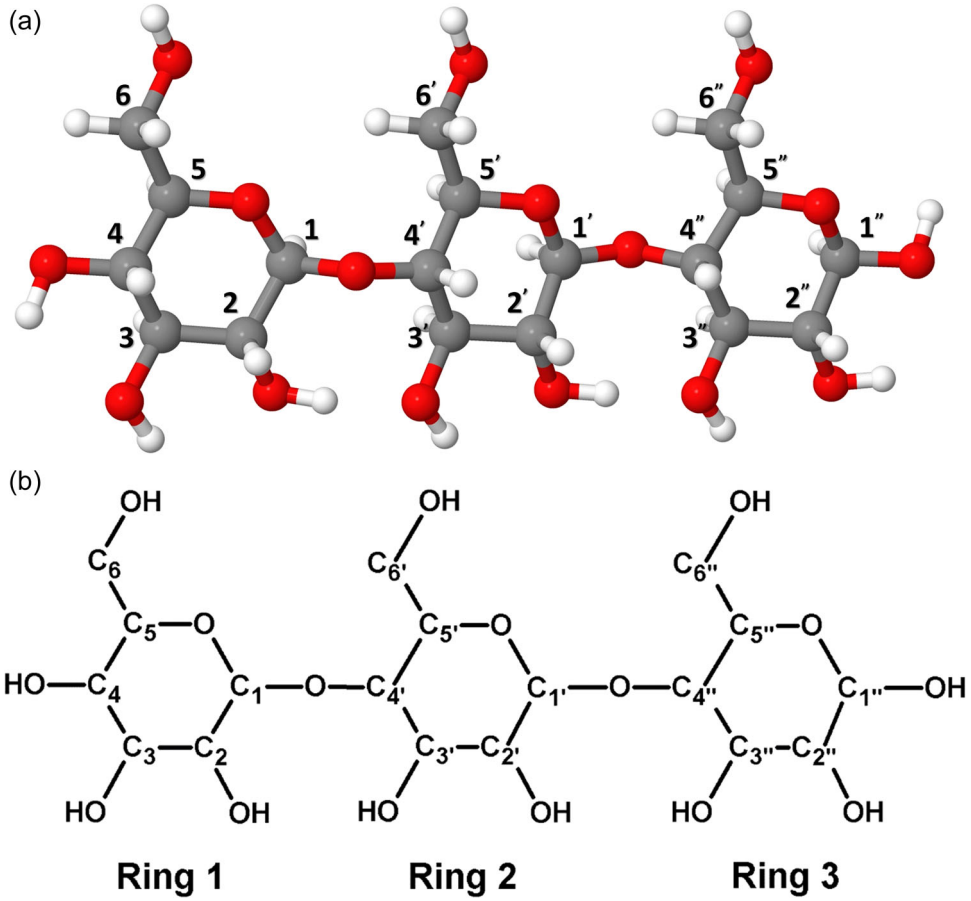

FIGURE 1 Schematic representation (a) and chemical structure (b) of the cellotriose molecule consisting of three β-D-glucose (gluc) units, that is, three rings. C, O, and H atoms in (a) are shown in gray, red, and white colors, respectively. The H atoms bound to the C atoms in (b) are not shown for clarity. The same applies to other similar figures below. All C atoms are numbered in the structure, which might participate in the interaction of O atoms with the system (see Table 2 below).

temperature (below 40°C) makes it of particular interest to treat not only bacteria or biofilms but also living tissues sensitive to heat and pressure (see e.g.,[51]).

Mass spectrometry (MS) experiments were carried out using a Q-TOF Synapt G2 HDMS T-wave ion mobility mass spectrometer with gold-coated borosilicate glass capillaries for static nano-electrospray ionization in positive polarity. Samples were introduced at a concentration of 5 μM and the capillary voltage was set at 1.6 kV and the sampling cone voltage at 20 V. Source and desolvation temperatures were set to 50 and 150°C, respectively. The mass range for detection was set at 100–2000 Da. Calibration of the instrument was performed by using a NaI/CsI solution.

Cellotriose solution with a concentration of 0.05% (w/v %) (500 μM in UPLC water) was treated by the plasma jet. Cellotriose was detected as $M+Na^+$ ions at *m/z* 527.16 (Table 1). After CAP treatment, additional oxidation products of the trisaccharide were observed with signals for $(M+O)+Na^+$, $(M+2O)+Na^+$ and $(M+3O)+Na^+$. Four additional oxidation products were observed in the low *m/z* range, corresponding to the disaccharide $M+Na^+$ and its oxidized products $(M+O)+Na^+$, $(M+2O)+Na^+$ and $(M+3O)+Na^+$, respectively (see Table 1). These signals refer to the loss of a glucose monomer from the intact trisaccharide and imply the cleavage of glycosidic bonds in the cellotriose (see next section). In addition, the mass spectra showed the presence of the corresponding monomeric glucose $(M+Na^+)$ at *m/z* 203.05 and its oxidized product $(M+O)+Na^+$ at m/z 219.04 (see Table 1). Next to the oxidation products with addition of extra oxygen atoms to the molecule, the mass spectra showed also signals corresponding to the oxidation of alcohols to carbonyl groups, such as like $(M-4H)+Na^+$ and $(M-2H)+Na^+$ and the corresponding oxidation products of these trisaccharides (Table 1). Analogous oxidation products were also found for the oxidized disaccharide. The signal at *m/z* 301.14 is believed to be a contamination of dibutylphtalate (i.e., a plasticizer).

	Compound	*m/z*		Compound	*m/z*
Trisaccharide	$M+Na^+$	527.16	Disaccharide	$M+Na^+$	365.05
	$(M+O)+Na^+$	543.16		$(M+O)+Na^+$	381.05
	$(M+2O)+Na^+$	559.16		$(M+2O)+Na^+$	397.05
	$(M+3O)+Na^+$	575.16		$(M+3O)+Na^+$	413.05
	$(M-4H)+Na^+$	523.13			
	$(M-2H)+Na^+$	525.14	Monosaccharide	$M+Na^+$	203.05
	$(M-4H)+O)+Na^+$	539.13		$(M+O)+Na^+$	219.04
	$(M-2H)+O)+Na^+$	541.14			
	$(M-4H)+2O)+Na^+$	555.14			
	$(M-2H)+2O)+Na^+$	557.14			
	$(M-4H)+3O)+Na^+$	573.14			
	$(M-2H)+3O)+Na^+$	575.14			

TABLE 1 Overview of observed compounds and their *m/z* in the treated cellotriose

4 | RESULTS AND DISCUSSION

As mentioned in the simulation details section, we performed DFTB-MD simulations for the interaction of O atoms (as the most reactive ROS) with the cellotriose molecule (Figure 1), to gain a better understanding of the oxidation process and the molecular mechanisms for this trisaccharide. In total 100 DFTB-MD simulations (i.e., 100 O atom impacts) were performed, from which we observed 40 reaction mechanisms that are summarized in Table 2. The relative occurrence of each specific reaction is displayed in column 3 of Table 2.

Our simulation results showed that all reactions are initiated by H-abstraction from a specific position on cellotriose. In other words, the O atom abstracts an H atom (or in some cases two H atoms) from the structure (see Figure 1), leading to further dissociation or the formation of some bonds. One of the most often observed reaction mechanisms (i.e., reaction 23 in Table 2) is illustrated in Figure 2. The O atom abstracts an H atom from the alcohol group bound to $C_{6'}$ (see red dashed arrow), leading to the formation of two radicals, that is, $C_{6'}$-$O^{\bullet}$ and $^{\bullet}OH$. Subsequently, these two radicals bind with each other, forming a new OH group in the system.

Note that the formed OOH group in Ring 2 is not necessarily stable, that is, it can revert back, but radical molecules also notoriously rearrange, eliminate or fragment in the following steps until more stable radicals are formed. Since we did not study the consecutive impacts of O atoms in our simulations, the subsequent reactions are likely to occur, thereby forming a stable structure. These "first step" reactions assist to unravel the onset of the reaction mechanisms, which are highly inaccessible to be studied by experimental observations. This type of reaction mechanism (i.e., H-abstraction and subsequent binding of OH) can also occur in other positions of the cellotriose molecule and was the most often observed reaction mechanism in our simulations (see reactions 1–24 in Table 2). It is obvious that this reaction mechanism eventually leads to the addition of an extra O atom to the system (+16 Da), which is in line with our experimental results (i.e., cellotriose +16 Da). Indeed, the results of mass spectrometry of CAP-treated cellotriose showed the addition of extra O atoms to the molecule (i.e., formation of OH groups); see Figure 3.

The addition of an extra O atom was also observed in D-glucose oxidation by CAP.[22] It was shown that the D-gluconic acid is the most abundant oxidation product (i.e., glucose + 16 Da) detected after plasma treatment.[22] Note that our simulations did not predict the experimentally observed structure with two or three additional O atoms, since we did not study the consecutive impacts of O atoms in our simulations. However, it is more likely that O addition (i.e., a new OH group formation) might take place subsequently at different positions of the system and this might lead to the formation of the above-mentioned structures. We also observed other reaction mechanisms, namely the reactions 25–38 in Table 2, which can lead to the formation of aldehyde or ester, or ketone groups, where the O atom abstracts two H atoms at the same time from the system (i.e., cellotriose −2 Da, see Figure 4). It should be mentioned here that the more obvious reaction of an aldehyde or ketone formation is that both hydrogens are abstracted from the same carbon and its OH group (reactions 29–32), rather than two adjacent events with ring opening (e.g., Figure 4). This indicates that we need to consider the relative occurrence

TABLE 2 Overview of all the reaction events observed in the simulations after the interaction of O atoms with cellotriose

No.	H-abstraction	Number of events	Consequence of reaction
1	C_1'	1	$C_{1'}$-OH is formed (+16 Da) no destruction of cellotriose
2	C_4'	2	$C_{4'}$-OH is formed (+16 Da) no destruction of cellotriose
3	C_5	1	C_5-OH is formed (+16 Da) no destruction of cellotriose
4	C_5'	**4**	$C_{5'}$-OH is formed (+16 Da) no destruction of cellotriose
5	$C_{5''}$	3	$C_{5''}$-OH is formed (+16 Da) no destruction of cellotriose
6	$C_{1''}$	**4**	$C_{1''}$-OH is formed (+16 Da) no destruction of cellotriose, formation of geminal diol (i.e., two OH groups linked to $C_{1''}$) → can be converted to ketone
7	C_2	1	additional C_2-OH is formed (+16 Da) no destruction of cellotriose, formation of geminal diol (i.e., two OH groups linked to C_2) → can be converted to ketone
8	C_2'	2	additional $C_{2'}$-OH is formed (+16 Da) no destruction of cellotriose, formation of geminal diol (i.e., two OH groups linked to $C_{2'}$) → can be converted to ketone
9	C_3	2	additional C_3-OH is formed (+16 Da) no destruction of cellotriose, formation of geminal diol (i.e., two OH groups linked to C_3) → can be converted to ketone
10	C_3'	2	additional $C_{3'}$-OH is formed (+16 Da) no destruction of cellotriose, formation of geminal diol (i.e., two OH groups linked to $C_{3'}$) → can be converted to ketone
11	$C_{3''}$	2	additional $C_{3''}$-OH is formed (+16 Da) no destruction of cellotriose, formation of geminal diol (i.e., two OH groups linked to $C_{3''}$) → can be converted to ketone
12	C_4	2	additional C_4-OH is formed (+16 Da) no destruction of cellotriose, formation of geminal diol (i.e., two OH groups linked to C_4) → can be converted to ketone
13	C_6	**5**	additional C_6-OH is formed (+16 Da) no destruction of cellotriose, formation of geminal diol (i.e., two OH groups linked to C_6) → can be converted to aldehyde
14	C_6'	**4**	additional $C_{6'}$-OH is formed (+16 Da) no destruction of cellotriose, formation of geminal diol (i.e., two OH groups linked to $C_{6'}$) → can be converted to aldehyde
15	$C_{6''}$	**4**	additional $C_{6''}$-OH is formed (+16 Da) no destruction of cellotriose, formation of geminal diol (i.e., two OH groups linked to $C_{6''}$) → can be converted to aldehyde
16	$C_{1''}$OH	3	$C_{1''}$O-OH is formed (+16 Da) no destruction of cellotriose
17	C_2OH	2	C_2O-OH is formed (+16 Da) no destruction of cellotriose
18	C_2'OH	1	$C_{2'}$O-OH is formed (+16 Da) no destruction of cellotriose

(Continues)

TABLE 2 (Continued)

No.	H-abstraction	Number of events	Consequence of reaction
19	$C_{2''}OH$	**5**	$C_{2''}O$-OH is formed (+16 Da) no destruction of cellotriose
20	C_3OH	**6**	C_3O-OH is formed (+16 Da) no destruction of cellotriose
21	$C_{3''}OH$	1	$C_{3''}O$-OH is formed (+16 Da) no destruction of cellotriose
22	C_6OH	**5**	C_6O-OH is formed (+16 Da) no destruction of cellotriose
23	$C_{6'}OH$	**9**	$C_{6'}O$-OH is formed (+16 Da) no destruction of cellotriose
24	$C_{6''}OH$	**5**	$C_{6''}O$-OH is formed (+16 Da) no destruction of cellotriose
25	C_3OH and C_4OH	**7**	C_3-C_4 bond is broken, $C_3=O$ and $C_4=O$ are formed (−2 Da) opening of Ring 1, but no glycosidic bond cleavage (aldehyde formation)
26	C_2OH and C_3OH	2	C_2-C_3 bond is broken, $C_2=O$ and $C_3=O$ are formed (−2 Da) opening of Ring 1, but no glycosidic bond cleavage (aldehyde formation)
27	$C_{2'}OH$ and $C_{3'}OH$	1	$C_{2'}$-$C_{3'}$ bond is broken, $C_{2'}=O$ and $C_{3'}=O$ are formed (−2 Da) opening of Ring 2, but no glycosidic bond cleavage (aldehyde formation)
28	$C_{2''}OH$ and $C_{3''}OH$	1	$C_{2''}$-$C_{3''}$ bond is broken, $C_{2''}=O$ and $C_{3''}=O$ are formed (−2 Da) opening of Ring 3, but no glycosidic bond cleavage (aldehyde formation)
29	$C_{1''}$ and $C_{1''}OH$	1	$C_{1''}=O$ is formed (−2 Da) no destruction of cellotriose (ester formation)
30	$C_{2'}$ and $C_{2'}OH$	1	$C_{2'}=O$ is formed (−2 Da) no destruction of cellotriose (ketone formation)
31	C_4 and C_4OH	1	$C_4=O$ is formed (−2 Da) no destruction of cellotriose (ketone formation)
32	$C_{6'}$ and $C_{6'}OH$	1	$C_{6'}=O$ is formed (−2 Da) no destruction of cellotriose (aldehyde formation)
33	C_1 and C_2OH	2	C_1-C_2 is broken (−2 Da) opening of Ring 1, but no glycosidic bond cleavage, aldehyde and carbene O-(:C_1)-O formation → carbonate ester group can be formed (+14 Da)
34	$C_{1''}$ and $C_{2''}OH$	1	$C_{1''}$-$C_{2''}$ is broken (−2 Da) opening of Ring 3, but no glycosidic bond cleavage, aldehyde and carbene O-(:$C_{1''}$)-O formation → carbonate ester group can be formed (+14 Da)
35	$C_{4'}$ and $C_{3'}OH$	1	$C_{4'}$-$C_{3'}$ is broken (−2 Da) opening of Ring 2, but no glycosidic bond cleavage, aldehyde and carbene O-(:$C_{4'}$)-$C_{5'}$ formation → carboxylate ester group can be formed (+14 Da)
36	C_5 and C_4OH	1	C_4-C_5 bond is broken (−2 Da) opening of Ring 1, but no glycosidic bond cleavage, aldehyde and carbene C_6-(:C_5)-O formation → carboxylate ester group can be formed (+14 Da)
37	C_3 and C_2OH	1	C_1-C_2 bond is broken, new C_1-C_3 bond is formed (−2 Da) shrinking of Ring 1, but no glycosidic bond cleavage (aldehyde formation)
38	$C_{4''}$ and $C_{6''}OH$	1	$C_{5''}$-$C_{6''}$ bond is broken (detachment of formaldehyde), $C_{4''}=C_{5''}$ bond is formed (-2 Da) no glycosidic bond cleavage, cellotriose -32 Da
39	$C_{2'}$and (*)	1	$C_{1'}$-O is broken, $C_{1'}=C_{2'}$ and $C_{4''}$O-OH are formed (glycosidic bond cleavage)

TABLE 2 (Continued)

No.	H-abstraction	Number of events	Consequence of reaction
			detachment of Ring 3, that is, glucose monomer +16 Da and disaccharide −18 Da formation
40	C_2 and (**)	1	C_1-O is broken, $C_1=C_2$ and $C_{4'}$O-OH are formed (glycosidic bond cleavage) detachment of Ring 1, that is, disaccharide +16 Da formation
TOTAL		100	

Note: For the meaning of the numbering of the various C atoms, see Figure 1 above. Note that all these reactions are initiated by H-abstraction, but the latter can occur at different C atoms or O atoms, as indicated by the second column. The consequences of the reactions are denoted by blue words in the last column. The formation of a glucose monomer or a disaccharide with an extra O atom (i.e., +16 Da) is indicated by red words. **Reactions 1–15**: The impinging O atom abstracts an H atom from the CH (or CH_2) group, resulting in the formation of two radicals, that is, $^{\bullet}$OH and C$^{\bullet}$ (or CH$^{\bullet}$); subsequently, these two radicals bind with each other, creating a new OH group in the system (see the last column).**Reactions 16–24**: The impinging O atom abstracts an H atom from the CH_x-OH group, resulting in the formation of two radicals, that is, $^{\bullet}$OH and CH_x-O$^{\bullet}$; subsequently, these two radicals bind with each other, creating a new OH group in the system (see the last column).**Reactions 25–28**: The impinging O atom abstracts H atoms from two CH-OH groups, leading to the formation of a water molecule and two CH-O$^{\bullet}$ radicals; this subsequently results in a breaking of the C-C bond and the formation of aldehyde groups (see the last column).**Reactions 29–32**: The impinging O atom abstracts H atoms from the CH (or CH_2) group and the OH group bound to it, leading to the formation of a water molecule and two radicals, that is, $^{\bullet}$O and C$^{\bullet}$ (or CH$^{\bullet}$); this subsequently results in the formation of an ester or ketone or aldehyde group (see the last column).**Reactions 33–38**: The impinging O atom abstracts H atoms from the CH group and CH_x-OH group, leading to the formation of a water molecule and two radicals, that is, C$^{\bullet}$ and $^{\bullet}$O; this subsequently results in the breaking of a C-C bond, followed by either ring opening (or shrinking) or detachment of formaldehyde from the system (see the last column).**Reactions 39–40**: The impinging O atom abstracts H atoms from the CH group, leading to the formation of an $^{\bullet}$OH radical; subsequently, this radical binds to the oxygen of the glycosidic bond (see * and ** below), resulting in the breaking of a glycosidic bond in the system (see the last column).*: Binding to the oxygen of the glycosidic bond $C_{1'}$-O-$C_{4''}$.**: Binding to the oxygen of the glycosidic bond C_1-O-$C_{4'}$

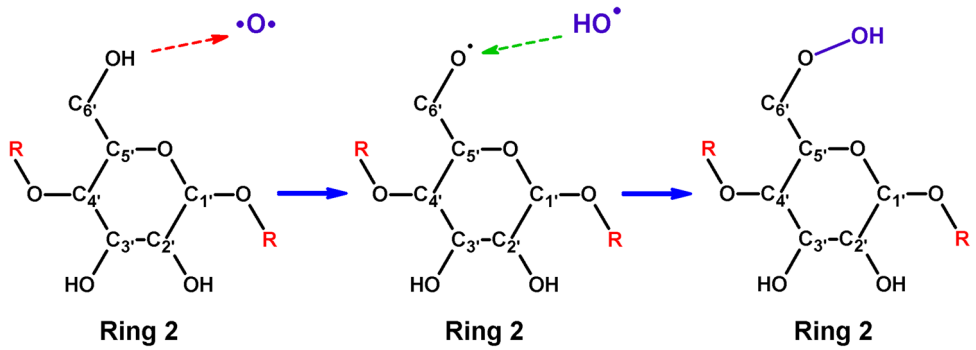

FIGURE 2 Illustration of the reaction mechanism where an O atom interacts with Ring 2 of the cellotriose (cf. Figure 1), leading to the formation of an additional OH group in the system (i.e., cellotriose + 16 Da). The H-abstraction and OH addition reactions are indicated by red and green dashed arrows, respectively.

of each reaction given in Table 2 with caution, because of the limited statistics, and it is more likely that the aldehyde or ketone formation reaction described above might actually take place, rather than ring opening.

In some of the reaction mechanisms we can see the radical sites left behind by the H-abstraction reaction (see reactions 33–36) and these radicals can further react with a new O atom, thereby forming carbonate or carboxylate ester groups (see Figure 5), eventually leading to the formation of the experimentally observed structure +14 Da (see red stars in Figure 3b). Again, as mentioned above, we did not study consecutive impacts of O atoms, for the sake of calculation time, but from our current simulations and from experiments [22,23] it is quite obvious that this further reaction is well possible.

Another reaction mechanism, that is, reaction 40 in Table 2, is shown in Figure 6. This reaction mechanism is important, as it leads to the dissociation of a glycosidic bond, as well as the formation of a disaccharide with an additional O atom, which is also observed in our experiments. Indeed, the experiments revealed that plasma treatment of cellotriose leads to a loss of a glucose monomer from the intact trisaccharide (see red and green areas in Figure 3a), suggesting the cleavage of glycosidic bonds in the oligosaccharide.

As mentioned above, the formed OOH group in Ring 2 is not necessarily stable and further reactions might occur to form stable products. Thus, the emphasis in this study is on the initial products, since we cannot realistically predict the final products observed in our

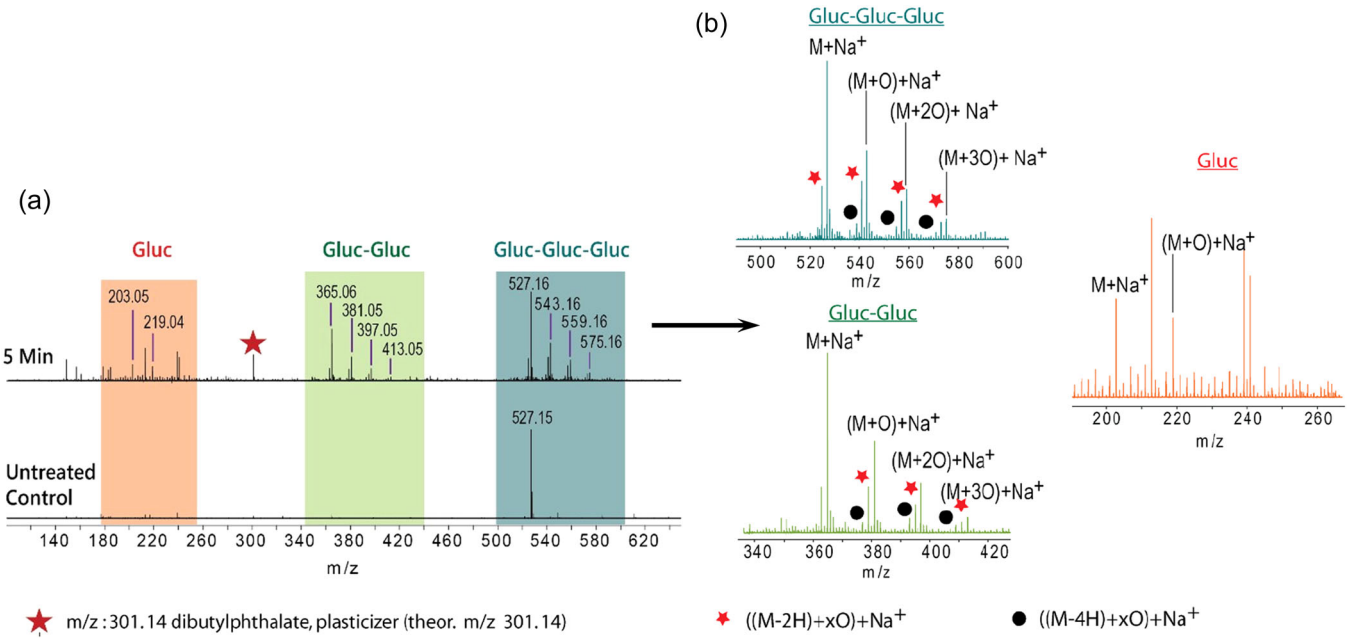

FIGURE 3 (a) Mass spectra of plasma-treated cellotriose trisaccharide (5 min) and untreated control. The areas highlighted in red, green, and blue correspond to monosaccharide (gluc), disaccharide (gluc-gluc), and trisaccharide (gluc-gluc-gluc), respectively. (b) Zoom-in on the mass range of trisaccharide (490–600 Da, blue), disaccharide (330–430 Da, green), and monosaccharide (190–270 Da, red) for 5 min treatment, clearly showing the addition of extra O atoms to the molecule.

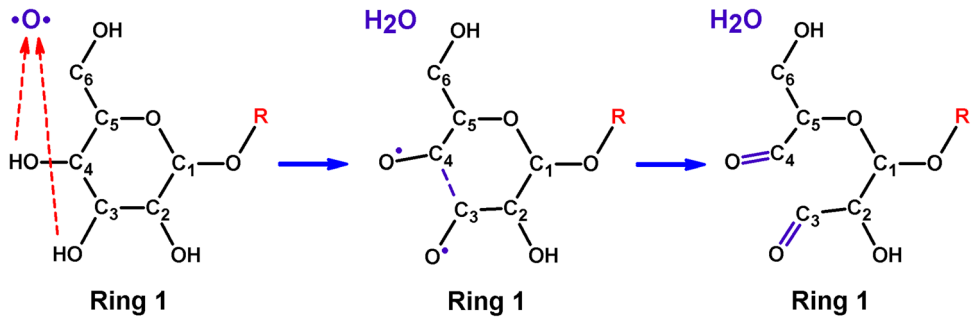

FIGURE 4 Reaction mechanism where two H atoms are abstracted from Ring 1 of the cellotriose (cf. Figure 1) by an impinging O atom, leading to the formation of a water molecule and aldehyde groups, as well as the breakage of the C_3-C_4 bond (i.e., cellotriose −2 Da). The H-abstraction reactions are indicated by red dashed arrows.

mass spectrometry measurements. Still, our computational results are fairly in line with the results of our experiments. Note that the relative occurrence of reaction 40 (see Table 2) in our simulations is very low (i.e., only 1%), although we need to consider this percentage with caution, due to the limited statistics, and the fact that we only performed single O atom impact runs in our simulations. It is clear from Figure 6 that the impinging O atom simultaneously abstracts an H atom bound to C_2 and binds to an O atom in the glycosidic bond between Ring 1 and Ring 2. This in turn leads to the formation of a $C_1 = C_2$ double bond and the dissociation of the C_1–$OC_{4'}$ glycosidic bond, as well as the formation of a new OH group in the disaccharide.

Similar to reaction 40, the mechanism of reaction 39 also leads to the breaking of the glycosidic bond and the formation of glucose with an additional O atom, observed in the mass spectra (see Figure 3b). Hence, the last two reaction mechanisms (see Table 2) eventually result in the dissociation of the glycosidic bond and formation of either a disaccharide +16 Da or glucose +16 Da structure, although an intact cellotriose molecule can also be observed by mass spectrometry after 5 min treatment (see Figure 3).

In general, our reactive DFTB-MD simulation results confirm the available experimental and modeling outcomes on plasma oxidation of different oligosaccharides,[21–35] and are also in line with experimental data of the CAP effect on the cellotriose molecule.

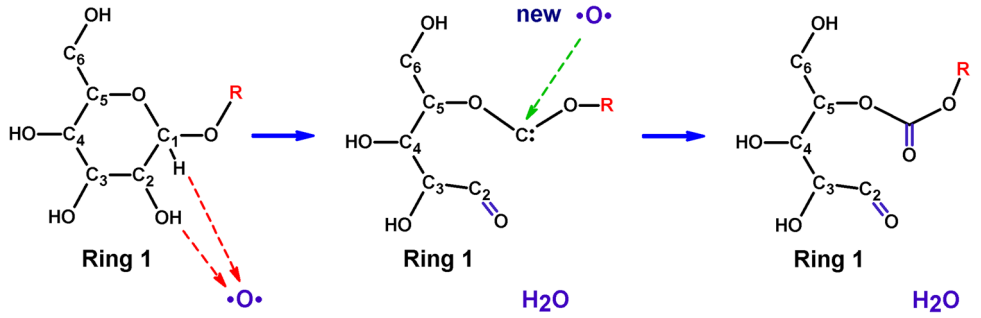

FIGURE 5 The mechanism of reaction 33 (see Table 2) where two H atoms are abstracted from Ring 1 of the cellotriose by an impinging O atom, leading to the breakage of the C_1-C_2 bond, as well as the formation of a water molecule, a C_2=O aldehyde group and an O-(:C_1)-O carbene molecule. A new O atom can further react with a carbene, thereby forming a carbonate ester group (i.e., cellotriose + 14 Da). The H-abstraction and new O addition reactions are indicated by red and green dashed arrows, respectively.

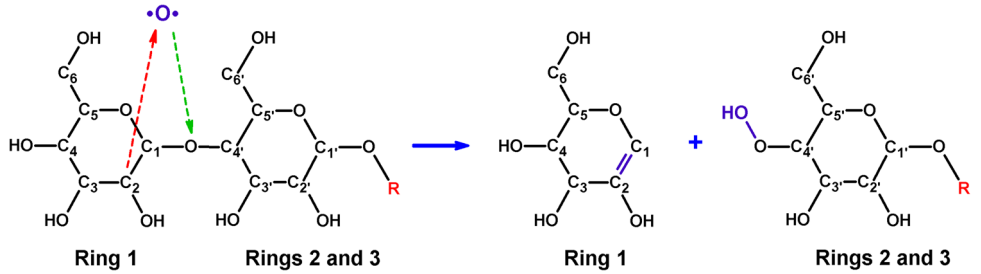

FIGURE 6 The glycosidic bond cleavage mechanism between Rings 1 and 2 upon impact of an O atom, leading to the formation of a disaccharide + 16 Da, as well as a monosaccharide with lower mass. The H-abstraction and OH addition reactions are indicated by red and green dashed arrows, respectively.

5 | CONCLUSIONS

In this study, we showed how DFTB-MD simulation results may help to gain more insight into the underlying mechanisms of the effect of CAP-generated ROS on oligosaccharides, thereby improving our understanding of the role of cold plasma in the treatment of biofilms. In particular, our simulation results reveal that the oxidation of cellotriose by O atoms can result in formation of OH groups, ring opening in monomers, as well as the dissociation of glycosidic bonds between glucose units, which subsequently leads to the disruption of the oligosaccharide.

Our DFTB-MD simulation results are in agreement with experimental work, where the cleavage of glycosidic bonds in cellotriose oligosaccharide, was observed due to CAP oxidation. Thus, our simulation results support and elucidate the experimental observations on the oxidation and glycosidic bond cleavage caused by plasma treatment.

ACKNOWLEDGMENTS

They also acknowledge the Turing HPC infrastructure at the CalcUA core facility of the University of Antwerp (UA), a division of the Flemish Supercomputer Center VSC, funded by the Hercules Foundation, the Flemish Government (department EWI), and the UA, where all computational work was performed. This study was financially supported by the Research Foundation–Flanders (FWO) (grant number 1200219N).

CONFLICT OF INTEREST

The authors declare no conflict of interest.

DATA AVAILABILITY STATEMENT

No data.

ORCID

Maksudbek Yusupov http://orcid.org/0000-0003-4591-858X

REFERENCES

[1] M. Abdallah, C. Benoliel, D. Drider, P. Dhulster, N.-E. Chihib, *Arch. Microbiol.* **2014**, *196*, 453.
[2] A. Vertes, V. Hitchins, K. S. Phillips, *Anal. Chem.* **2012**, *84*, 3858.
[3] D. Estivill, A. Arias, A. Torres-Lana, A. J. Carrillo-Muñoz, M. P. Arévalo, *J. Microbiol. Methods* **2011**, *86*, 238.
[4] H.-S. Joo, M. Otto, *Chem. Biol.* **2012**, *19*, 1503.

[5] T. R. Garrett, M. Bhakoo, Z. Zhang, *Prog. Nat. Sci.* **2008**, *18*, 1049.
[6] H.-C. Flemming, T. R. Neu, D. J. Wozniak, *J. Bacteriol.* **2007**, *189*, 7945.
[7] A. Mai-Prochnow, M. Bradbury, K. Ostrikov, A. B. Murphy, *PLoS One* **2015**, *10*, e0130373.
[8] A. Mai-Prochnow, *Chapter 4-Cold Plasma to Control Biofilms on Food and in the Food-Processing Environment*, Academic Press, **2020**.
[9] A. Mai-Prochnow, R. Zhou, T. Zhang, K. K. Ostrikov, S. Mugunthan, S. A. Rice, P. J. Cullen, *NPJ Biofilms Microbio.* **2021**, *7*, 1.
[10] S. Khosravi, S. Jafari, H. Zamani, M. Nilkar, *Appl. Biochem. Biotechnol.* **2021**, *193*, 3641.
[11] G. Nima, E. Harth-Chu, R. D. Hiers, V. G. A. Pecorari, D. W. Dyer, S. S. Khajotia, M. Giannini, F. L. E. Florez, *Sci. Rep.* **2021**, *11*, 23800.
[12] D. Lahiri, S. Dash, R. Dutta, M. Nag, *J. Biosci.* **2019**, *44*, 52.
[13] H. Tanhay Mangoudehi, H. Zamani, S. S. Shahangian, L. Mirzanejad, *World J. Microbiol. Biotechnol.* **2020**, *36*, 70.
[14] X. Pei, X. Lu, J. Liu, D. Liu, Y. Yang, K. Ostrikov, P. K. Chu, Y. Pan, *J. Phys. D: Appl. Phys.* **2012**, *45*, 165205.
[15] P. Bourke, D. Ziuzina, L. Han, P. J. Cullen, B. F. Gilmore, *J. Appl. Microbiol.* **2017**, *123*, 308.
[16] T. von Woedtke, A. Kramer, *GMS Krankenhhyg. Interdiszip.* **2008**, *3*, 19.
[17] T. von Woedtke, A. Kramer, K.-D. Weltmann, *Plasma Processes Polym.* **2008**, *5*, 534.
[18] J. Feichtinger, A. Schulz, M. Walker, U. Schumacher, *Surf. Coat. Technol.* **2003**, *174-175*, 564.
[19] M. K. Boudam, M. Moisan, B. Saoudi, C. Popovici, N. Gherardi, F. Massines, *J. Phys. D: Appl. Phys.* **2006**, *39*, 3494.
[20] D. Soignet, O. Hinojosa, T. Ward, R. Benerito, *J. Macromol. Sci. Chem.* **1982**, *17*, 403.
[21] Y. Li, G. Friedman, A. Fridman, H.-F. Ji, *Clin. Plas. Med.* **2014**, *2*, 56.
[22] M. Ahmadi, Z. Nasri, T. von Woedtke, K. Wende, *ACS Omega* **2022**, *7*, 28361.
[23] J. Benedikt, M. Mokhtar Hefny, A. Shaw, B. R. Buckley, F. Iza, S. Schäkermann, J. E. Bandow, *Phys. Chem. Chem. Phys.* **2018**, *20*, 12037.
[24] F. D. L. Almeida, R. S. Cavalcante, P. J. Cullen, J. M. Frias, P. Bourke, F. A. Fernandes, S. Rodrigues, *Innovative Food Sci. Emerg. Technol.* **2015**, *32*, 127.
[25] J. Delaux, C. Ortiz Mellet, C. Canaff, E. Fourré, C. Gaillard, A. Barakat, J. M. García Fernández, J.-M. Tatibouët, F. Jérôme, *Chem. A Eur. J.* **2016**, *22*, 16522.
[26] M. Yusupov, E. Neyts, U. Khalilov, R. Snoeckx, A. Van Duin, A. Bogaerts, *New J. Phys.* **2012**, *14*, 093043.
[27] M. Yusupov, A. Bogaerts, S. Huygh, R. Snoeckx, A. C. Van Duin, E. C. Neyts, *J. Phys. Chem. C* **2013**, *117*, 5993.
[28] M. Yusupov, E. C. Neyts, C. C. Verlackt, U. Khalilov, A. C. Van Duin, A. Bogaerts, *Plasma Processes Polym.* **2015**, *12*, 162.
[29] A. Bogaerts, M. Yusupov, J. Van der Paal, C. C. Verlackt, E. C. Neyts, *Plasma Processes Polym.* **2014**, *11*, 1156.
[30] N. Khosravian, A. Bogaerts, S. Huygh, M. Yusupov, E. C. Neyts, *Biointerphases* **2015**, *10*, 029501.
[31] T. Zhao, L. Shi, Y. Zhang, L. Zou, L. Zhang, *Phys. Plasmas* **2017**, *24*, 103518.
[32] J. Cui, T. Zhao, L. Zou, X. Wang, Y. Zhang, *J. Phys. D: Appl. Phys.* **2018**, *51*, 355401.
[33] X. Wang, L. Pang, S. Yang, L. Zou, Y. Zhang, T. Zhao, *Biochem. Biophys. Res. Commun.* **2021**, *576*, 53.
[34] S. Yang, T. Zhao, J. Cui, Z. Han, L. Zou, X. Wang, Y. Zhang, *Plasma Sci. Technol.* **2020**, *22*, 125401.
[35] H. Yin, G. Gao, Y. Yang, K. Liu, G. Wu, *Phys. Plasmas* **2022**, *29*, 033508.
[36] M. Yusupov, A. Privat-Maldonado, R. M. Cordeiro, H. Verswyvel, P. Shaw, J. Razzokov, E. Smits, A. Bogaerts, *Redox Biol.* **2021**, *43*, 101968.
[37] K. A. Kristiansen, M.Ø. Dalheim, B. E. Christensen, *Pure Appl. Chem.* **2013**, *85*, 1893.
[38] M. K. Cowman, *Chapter One - Hyaluronan and Hyaluronan Fragments*, 74, Academic Press, **2017**.
[39] A. H. Pandit, N. Mazumdar, S. Ahmad, *Int. J. Biol. Macromol.* **2019**, *137*, 853.
[40] M. Elstner, D. Porezag, G. Jungnickel, J. Elsner, M. Haugk, T. Frauenheim, S. Suhai, G. Seifert, *Phys. Rev. B: Condens. Matter Mater. Phys.* **1998**, *58*, 7260.
[41] M. Elstner, T. Frauenheim, S. Suhai, *J. Mol. Struct. Theochem* **2003**, *632*, 29.
[42] M. Gaus, A. Goez, M. Elstner, *J. Chem. Theory Comput.* **2013**, *9*, 338.
[43] H.-J. Qian, A. C. van Duin, K. Morokuma, S. Irle, *J. Chem. Theory Comput.* **2011**, *7*, 2040.
[44] M. Gaus, X. Lu, M. Elstner, Q. Cui, *J. Chem. Theory Comput.* **2014**, *10*, 1518.
[45] M. Kubillus, T. Kubar, M. Gaus, J. Rezac, M. Elstner, *J. Chem. Theory Comput.* **2015**, *11*, 332.
[46] M. M. Hefny, C. Pattyn, P. Lukes, J. Benedikt, *J. Phys. D: Appl. Phys.* **2016**, *49*, 404002.
[47] H. J. Berendsen, J.v Postma, W. F. Van Gunsteren, A. DiNola, J. R. Haak, *J. Chem. Phys.* **1984**, *81*, 3684.
[48] B. Aradi, B. Hourahine, T. Frauenheim, *J. Phys. Chem. A* **2007**, *111*, 5678.
[49] B. Hourahine, B. Aradi, V. Blum, F. Bonafé, A. Buccheri, C. Camacho, C. Cevallos, M. Deshaye, T. Dumitrică, A. Dominguez, *J. Chem. Phys.* **2020**, *152*, 124101.
[50] D. Ellerweg, J. Benedikt, A. von Keudell, N. Knake, V. Schulz-von der Gathen, *New J. Phys.* **2010**, *12*, 013021.
[51] S. Bekeschus, K. Wende, M. M. Hefny, K. Rödder, H. Jablonowski, A. Schmidt, T.v Woedtke, K.-D. Weltmann, J. Benedikt, *Sci. Rep.* **2017**, *7*, 2791.

How to cite this article: M. Yusupov, D. Dewaele, P. Attri, U. Khalilov, F. Sobott, A. Bogaerts, *Plasma Processes Polym.* **2023**;20:e2200137. https://doi.org/10.1002/ppap.202200137